www.sciencemag.org/cgi/content/full/1155559/DC1

Supporting Online Material for

Subnanometer Motion of Cargoes Driven by Thermal Gradients Along Carbon Nanotubes

Amelia Barreiro, Riccardo Rurali, Eduardo R. Hernández,* Joel Moser, Thomas Pichler, László Forró, Adrian Bachtold*

*To whom correspondence should be addressed.
E-mail: adrian.bachtold@cnm.es (A.B.); ehe@icmab.es (E.R.H.)

Published 10 April 2008 on *Science* Express

DOI: 10.1126/science.1155559

This PDF file includes:

Materials and Methods
Figs. S1 to S5
Tables S1 and S2
References

Other Supporting Online Material for this manuscript includes the following:
(available at www.sciencemag.org/cgi/content/full/1155559/DC1)

Movies S1 to S5

Online Supporting Material

Subnanometer Motion of Cargoes Driven by Thermal Gradients along Carbon Nanotubes

Amelia Barreiro, Riccardo Rurali, Eduardo R. Hernández, Joel Moser, Thomas Pichler, Laszlo Forro, Adrian Bachtold

Section A: AFM manipulation

We selectively evaporated the outermost shell of the MWNT by injecting a large current through it. This is the so-called electrical breakdown technique [1, 2, 3]. Previous works have shown that the outermost shell is removed along the entire portion between the voltage electrodes. Here, the device is slightly different since a gold plate was placed between the voltage electrodes on top of the MWNT, and we found that the outermost shell is not removed in the portion below this gold plate (see top schematic of Fig. S1). This can be inferred from the following AFM manipulations. The gold plate can be moved back and forth several times using an AFM tip, a few of these movements are shown in the AFM images in Fig. S1 and the whole sequence of movements is shown in video S1. In contrast, the devices that were not engineered with the electrical-breakdown technique did not allow for such a manipulation. The cargo stayed immobile until it was suddenly detached from the nanotube when the force applied by the tip became too large.

The reduced evaporation of the outermost shell below the gold plate is due to the fact that the plate acts as a heat sink, which dissipates away the excess heat generated in the nearby portion of the MWNT. The temperature is lower, which reduces the probability

of the outermost shells to be removed, and results in the moveable structure shown in the top schematic of Fig. S1.

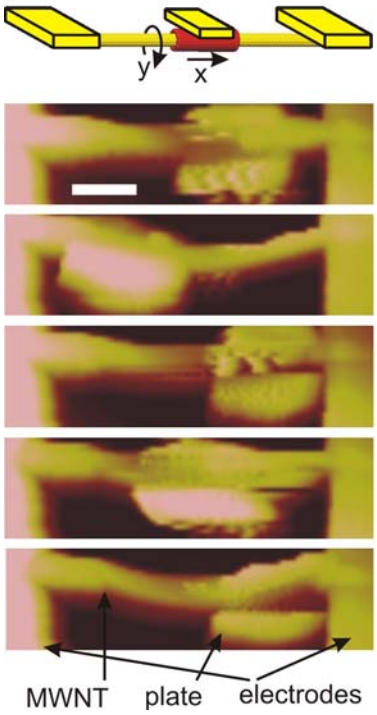

Fig. S1: AFM images of one device where the gold plate has been moved back and forth using an AFM tip. The scale bar is 300 nm. The image quality is poor due to the difficulty of imaging suspended structures.

Section B: Current actuation and statistics

The finding that the outermost shell of the MWNT is not removed below the gold plate (as shown in the top schematic of Fig. S1) is also supported by measurements where the motion of the gold plate is actuated by a current. Indeed, it is possible to move the gold plate for most of the engineered devices, while for non-engineered devices this is never the case (Table S1). Motion was observed for 84% of the engineered devices with a resistance lower than 700 kΩ. In contrast, 100% of the non-engineered devices remained immobile.

A few representative videos of the motion are included online. Video S2 shows the translation of a gold plate over 450 nm. Note that a few little back and forth rotations occur on top of the translation motion. Video S3 displays the stepwise rotation of a rectangular gold plate, while in video S4 a melted plate continuously rotates over more than 360 degrees. Note that videos S2-S4 are in real time, but video S3 was cut once, when the voltage was set to zero for a short period of time.

We emphasize that the rotation motion is not a result of the magnetic field induced by the current passing through the MWNT, since the rotation can be right-handed as well as left-handed with respect to the current flow (Table S1). Nor is the motion the result of a stray electric field, as the metal plate stays immobile for high-resistive devices (Table S1) even if a high voltage is applied. As discussed in the paper, the motion is driven by the thermal gradient along the nanotube, which is induced by the electrical current. This driving mechanism is consistent with the observation that the gold plate continues to move in the same direction upon reversing the electron current (video S2). This was seen in two different devices. The remaining devices deteriorated before the polarity inversion experiments could be carried out.

electrical breakdown	resistance	motion	description of motion
engineered	35 kΩ	YES	translation with back and forth rotation
engineered	36 kΩ	YES	left-hand rotation
engineered	43 kΩ	YES	left-hand rotation
engineered	45 kΩ	NO	
engineered	60 kΩ	YES	left-hand rotation, then translation
engineered	64 kΩ	YES	translation with back and forth rotation
engineered	78 kΩ	YES	right-hand rotation
engineered	94 kΩ	NO	
engineered	102 kΩ	YES	left-hand rotation
engineered	133 kΩ	YES	right-hand rotation
engineered	172 kΩ	YES	left-hand rotation
engineered	246 kΩ	YES	right-hand rotation
engineered	680 kΩ	YES	right-hand rotation
engineered	1 MΩ	NO	
engineered	1.2 MΩ	NO	
engineered	1.5 MΩ	NO	
non-engineered	13 kΩ	NO	
non-engineered	50 kΩ	NO	
non-engineered	53 kΩ	NO	
non-engineered	62 kΩ	NO	
non-engineered	78 kΩ	NO	

Table S1: Characteristics of the studied devices.

Section C: Velocity of the translational motion

For some devices such as in video S2, the motion can be rather continuous over several tens of nanometers before being blocked for some time at a specific position. This immobilisation of the metal plate is attributed to some dangling bonds or defects that obstruct the motion. Interestingly, the velocity changes along the length of the tube (Fig. S2). The velocity is maximum near the midpoint of the tube, where the temperature is highest, and is significantly reduced near the tube end. The velocity is therefore correlated to the temperature. However, more measurements need to be carried out for a quantitative analysis. Note that the value of the velocities near the tube midpoint is a lower bound (the motion occurs within one frame of the video).

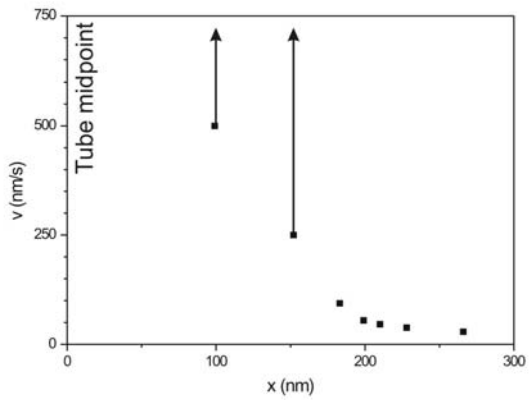

Fig. S2: Velocity as a function of the tube position. The origin of the x axis corresponds to the midpoint of the nanotube. The value of the velocity is a lower bound for the first points marked by an arrow. The measurements are obtained on a different tube from the one shown in video S2.

Section D: Melting of the plate

We often observed the gold plate to melt before it started to move. The initially rectangular shape transformed into a round ball (Fig. S3). The melting is attributed to the large current applied through the nanotube, which rises the temperature through Joule heating. The temperature can be inferred from the melting temperature of gold, which is about 1300 K.

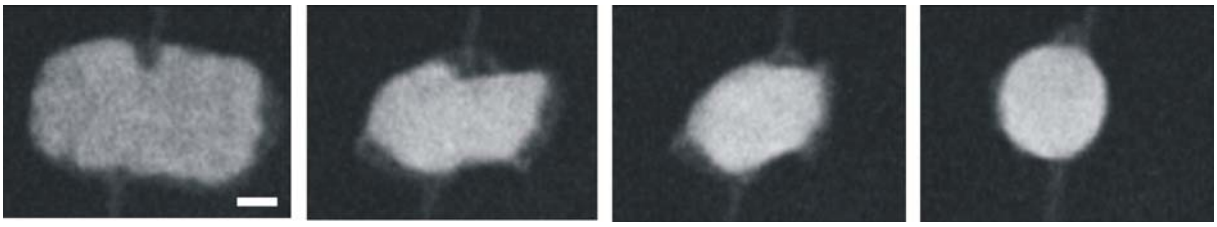

Figure S3: SEM images of one gold plate that is melting from left to right. The scale bar is 50 nm. The voltage applied between the electrodes is 3.3 V and the current 0.06 mA.

Section E: Molecular Dynamics Simulations

We conducted a series of molecular dynamics (MD) simulations of coaxial double-walled tubes imposing a thermal gradient along one of the nanotubes. We chose different combinations of tubes with the restriction that the difference in radii between inner and outer tube be compatible with the spacings experimentally observed in multi-walled nanotubes and graphite (c.a. 3.4 Angstrom). The inner tube was long, typically 100 nm, while the outer tube was shorter, having a length of approximately 5 nm, depending on the actual tube structure. In Fig. S4 we illustrate the geometry of one of our simulated systems consisting of an inner (17,0) nanotube, with a total length of 100.3 nm, and an outer (26,0) nanotube, of length 5.14 nm. This particular system consisted of a total of 17160 carbon atoms, 15912 in the inner tube, and 1248 in the

outer one. We label this particular system as (17,0)/(26,0). Details of other simulated systems are provided in table S2.

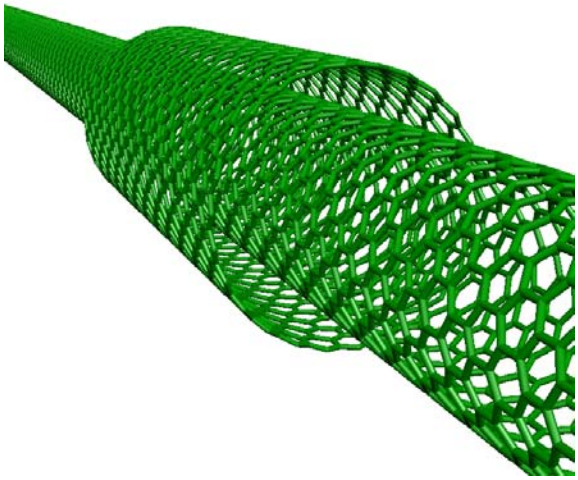

Figure S4: View of one of the double-walled nanotubes simulated. The outer tube is a 5.14 nm long (26,0) nanotube, and the inner one is a (17,0) nanotube with a length of 100.3 nm.

System	Length (nm)	Number of atoms
Inner tube / outer tube	Inner tube / outer tube	Inner tube / outer tube
(8,2)/(12,8)	100.2 / 5.6	8568 / 912
(8,2)/(17,2)	100.2 / 5.2	8562 / 872
(10,10)/(15,15)	99.9 / 4.95	16160 / 1200
(10,10)/(26,0)	99.9 / 5.14	16160 / 1248
(17,0)/(26,0)	100.3 / 5.14	15912 / 1248
(17,0)/(15,15)	100.3 / 4.95	15912 / 1200
(12,9)/(17,14)	99.0 / 7.7	16872 / 1928

Table S2: Details of the systems simulated with molecular dynamics.

Following Saito et al. [4], we have modelled the intra-tube interactions by means of the Tersoff potential [5], while the inter-tube interactions are described by means of a Lennard-Jones potential parametrized as in Ref. [4]. The extremities of the long inner tube are kept at two different temperatures by imposing the velocities of the atoms. One end (the cold one) was kept at a temperature of 300 K, while the hot end was maintained at a temperature chosen so as to impose the desired thermal gradient. The temperature gradients used were ~7, ~4 and ~1 K/nm, the latter one corresponding to the one estimated to occur in our experiments.

The equations of motion were integrated numerically using the velocity Verlet algorithm [6], with a time step of 2 fs. The thermal gradient was stabilised during a long run of 200 ps of the inner tube alone. This proved to be sufficiently long to produce a stable linear temperature gradient. In a separate run, the outer tube was also simulated on its own, but in the absence of any thermal gradient, in order to equilibrate it at room temperature. Initial atomic velocities were taken from the Maxell-Boltzmann distribution, making sure that the outer tube center of mass had no net velocity. Once both equilibration calculations were completed, the outer nanotube was placed at the mid-point of the inner tube, and production runs of the combined system were performed. Production simulations were then run for 200 to 400 ps.

In all cases we observed that the presence of a thermal gradient along the inner tube resulted in a net motion of the outer tube toward the cold end. In Fig. S5 we plot the position of the center of mass of the outer nanotube as a function of time for the system (12,9)/(17,14), obtained from simulations at three different thermal gradients. As can be seen in Fig. S5, at short times the displacement is small, since the outer nanotube is

initially at rest, and it takes some time for the thermal gradient to have a noticeable effect. Eventually, however, the displacement down the thermal gradient becomes appreciable, and the speed attained by the outer tube is larger the larger the thermal gradient.

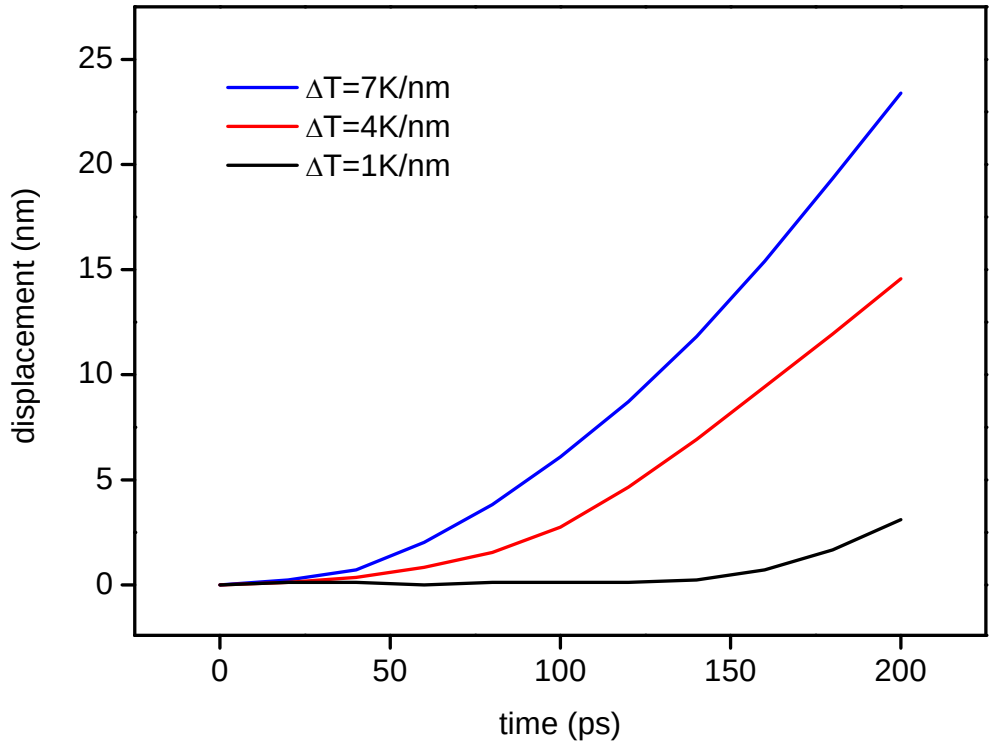

Figure S5: Displacements of the center of mass of the outer shell in the (12,9)/(17,14) tube system in different thermal gradients resulting from molecular dynamics simulations. The displacement is measured with respect to the initial position at the midpoint of the inner (12,9) tube along the tube axis. As can be seen, the displacements and the velocity of the center of mass is larger the larger the thermal gradient.

In video S5 we illustrate a sample trajectory for the (17,0)/(26,0) system, subject to a thermal gradient of 7 K/nm (three snapshots of this movie are shown in Fig. 4 of the accompanying paper). The movie spans a total time of 200 ps, and each frame is

separated by 20 ps from the previous one. The section of inner tube shown is approximately 30 nm long. The inner tube can be seen to oscillate and vibrate significantly along its length due to thermal energy, while the outer tube travels down the thermal gradient nearly 30 nm during the 200 ps of simulation. The existence of the thermal gradient implies an imbalance in the phonon populations at the hot and cold ends of the inner nanotube. This results in a net flow of phononic excitations travelling down the thermal gradient, which collide and transfer momentum to the outer tube, eventually resulting in a net displacement of the latter. This is in some sense the inverse process of the phononic contribution to friction: when two interfaces slide against each other, some of the kinetic energy is converted into lattice vibrations, and hence friction results in heating. Here, in contrast, we have a net flow of phononic excitations travelling from the hot side to the cold side. Some of the energy transported by these phononic excitations is converted into kinetic energy of the outer tube. The details of how this energy conversion occurs will be the subject of a future study.

References

[1] P.G. Collins, M. S. Arnold, Ph. Avouris, *Science* **292**, 706 (2001).

[2] P.G. Collins, M. Hersam, M. Arnold, R. Martel, Ph. Avouris, *Phys. Rev. Lett.* **86**, 3128 (2001).

[3] B. Bourlon, D.C. Glattli, B. Placais, J.M. Berroir, C. Miko, L. Forro, A. Bachtold, *Phys. Rev. Lett.* **92**, 26804 (2004).

[4] R. Saito, R. Matsuo, T. Kimura, G. Dresselhaus and M. S. Dresselhaus, *Chem. Phys. Lett.* **348**, 187 (2001).

[5] J. Tersoff, *Phys. Rev. Lett.* **61**, 2879 (1988).

[6] M. P. Allen and D. J. Tildesley, *Computer Simulation of Liquids* (Clarendon Press, Oxford 1987).

Movie Legends

Movie S1: Motion imaged by AFM

Movie S2: Translational motion

Movie S3: Stepwise rotational motion

Movie S4: 2π rotational motion

Movie S5: Simulated motion